Received: 28 September 2023 | Revised: 23 October 2023 | Accepted: 23 October 2023

DOI: 10.1002/jrs.6618

RESEARCH ARTICLE

Journal of RAMAN SPECTROSCOPY WILEY

Cluster approach for the density functional theory study of organic cation vibrations in hybrid halide post-perovskite 3-cyanopyridinium lead tribromide

Irina V. Krauklis | **Anna Yu Samsonova** | **Nikita I. Selivanov** | **Yury V. Kapitonov** | **Yuri V. Chizhov**

Saint Petersburg State University, St. Petersburg, Russia

Correspondence
Anna Yu Samsonova, Saint Petersburg State University, 7/9 Universitetskaya Emb., St. Petersburg 199034, Russia.
Email: sam5onowaa@yandex.ru

Funding information
Russian Science Foundation, Grant/Award Number: 22-22-00437

Abstract

Internal vibrations of organic cations in halide perovskites and their analogues could be used to study the crystal structure of these novel semiconductor materials. In this work, we have studied the vibration properties of the 3-cyanopyridinium ($3cp^+ = [3\text{-}CN\text{-}C5H5NH]^+$) cation in the hybrid organic–inorganic halide post-perovskite $(3cp)PbBr_3$. For DFT modeling of the experimental Raman spectrum, we have constructed three different models: free cation, minimal stoichiometric cluster and nanocluster. Calculations of a free cation adequately describe most of the internal vibrations. To describe high-wavenumber hydrogen stretching vibrations, and first of all N–H vibrations, it is necessary to use sufficiently large clusters. We show in the cluster approach for crystal field description that it is necessary to include in the cluster not only halogens but also their nearest environment. In this case, agreement with experiment is reached, and further considerations can be put forward about the strength of the hydrogen bond and its role in stabilising the crystal.

KEYWORDS

density functional theory, halide perovskites, hydrogen bond, Raman scattering

1 | INTRODUCTION

Halide perovskites and their low-dimensional analogues are unique ionic semiconductors with possible applications ranging from solar cells[1] to lasers[2,3] and from white light emitting diodes[4] to informational photonics elements.[5] This class of materials has a huge variety of crystal structures: in addition to the diversity of structures known for all-inorganic oxide perovskites, hybrid organic–inorganic halide perovskites exhibit a vast diversity of structures defined by organic cations. The most studied members of the latter are three-dimensional (3D) hybrid lead halide perovskites with the structural formula ABX_3 ($A^+ = CH_3NH_3^+$, HC $[NH_2]^+$; $B^{2+} = Pb^{2+}$, Sn^{2+}; $X^- = I^-$, Br^-, Cl^-).[6] Three-dimensional crystal structure is formed by the corner-shared lead-halide octahedra and small organic cations A^+ in the cavities formed by the octahedra framework.

Larger organic cations A^+ break classic 3D perovskite structure being able to stabilise 2D,[7,8] 1D,[9,10] and 0D[11] structures and more complex haloplumbates and analogues.[12–14] Among these low-dimensional perovskite-like structures quasi-2D crystals got great attention due to prospect optical features for the optoelectronic devices, such as broadband exciton emission, bandgap tuning and increased oscillator strength.[15–17]

The physical properties of perovskite materials depend dramatically on their crystal structure. One of the

research techniques that are able to address this structure is vibrational spectroscopy, namely infrared (IR) absorption and Raman scattering. Raman spectroscopy is actively used to study the vibrational properties of perovskite crystals[18,19] and thin films.[20,21] However, the large mass of the lead cation and halogen anions leads to low wavenumbers of the inorganic subsystem (below 200 cm^{-1}). This complicates the study of inorganic subsystem vibrations by widespread standard equipment. In predominantly ionic crystals of halide perovskites, organic cations remain sufficiently isolated. For this reason the observed internal vibrations of organic cations in the crystal correlate quite well with the vibrations of free cations lying in the 200–3500 cm^{-1} range.

The organic cations also could be treated as spectators of the crystalline environment. The crystalline environment has an effect on organic cations vibrations, which can manifest itself in (1) the polarisation of Raman lines due to the symmetry of the ordered arrangement of cations in the crystal; (2) splitting of lines due to a decrease in the symmetry of cations, the interaction of cations or the presence of several nonequivalent crystal sites; (3) shifts of lines due to the interaction of cations with the environment; and (4) changes in lines intensity including the emergence of vibrations prohibited in free cations by symmetry selection rules. Various internal vibrations are subject to these phenomena to varying degrees, and among them, the greatest influence can be expected for the vibrations of the N–H group holding the major positive charge of the cation.

Density functional theory (DFT) could be used to model vibrational spectra with two possible approaches. The first of them is the modeling of the whole crystal by the periodic DFT. This method faces several problems: the limited choice of available functionals, the long duration of calculations in the case of a large number of atoms in the unit cell (for example, crystals with reduced symmetry) and the complexity of interpreting observed effects. Another approach is the DFT calculations of crystal fragments (clusters) cut from the periodic crystal.[22,23] This method is attractive due to the possibility of a gradual transition from the isolated cation to the cation in the crystal environment. In halide perovskites the inter-cation interaction is minimal, and the masses of atoms of the inorganic subsystem are large and they can be considered practically stationary for calculations of internal vibrations of organic cations. For these reasons, one can expect a good agreement between the DFT calculation and experiment results even for rather small clusters.

In this work, we will sequentially construct a cluster, which will allow us to take into account the influence of the crystalline environment on the Raman spectra of an organic cation in a perovskite-like structure. As an object for study, we chose the halide post-perovskite 3-cyanopyridinium lead tribromide (3cp)$PbBr_3$ ($3cp^+$ = $[3–CN–C5H5NH]^+$).[24] This material belongs to the class of layered perovskite-like compounds with inorganic layers separated by layers of organic cations. The DFT was used earlier to address the properties of cations in this material. DFT of isolated cation was used to establish the vibrations selection rules and to identify vibrations in the Raman spectrum of the material.[25] The cluster consisting of two cations (dimer) was used to evaluate the inter-cation interaction manifesting itself as an emergence of the organic band in crystal DFT study.[24] In this work, we will study three different models and compare the obtained results with the experimental Raman spectrum.

2 | EXPERIMENTAL DETAILS

The synthesis and basic characterisation of (3cp) $PbBr_3$ post-perovskite single crystals are given in previous studies.[24,25] The experimental Raman spectrum of post-perovskite (3cp)$PbBr_3$ was measured at $T = 300$ K using a Horiba LabRam HR 800 spectrometer with a grating of 1800 mm^{-1} and a spectral resolution of 2 cm^{-1}. A solid-state laser with a wavelength of 532 nm and a power of 10 mW was used for sample excitation. The intensities, at which visible changes with the sample and spectrum occur, were found and several orders of magnitude less were chosen for recording the spectra. Also, the coincidence of the spectra at the beginning and end of the experiment was checked. To focus the laser beam on the surface of the sample, an Olympus BX41 microscope with an objective with a numerical aperture of (10×)/0.75 was used. The unpolarised Raman spectrum was recorded. A detailed study of polarised Raman spectra and the selection rules used for their interpretation is given in our recent paper.[25] DFT calculations were performed using the GAUSSIAN16 program[26] installed on the Huawei cluster in the Computing Center of St. Petersburg State University (cc.spbu.ru). The wB97XD functional was used with correction for long distances and taking into account dispersion interactions. The full def2SVP basis set available for heavy elements (Pb and Br) was used.

3 | RESULTS AND DISCUSSION

Figure 1 shows the experimental unpolarised Raman spectrum of (3cp)$PbBr_3$ single crystal. Due to the large mass of atoms that make up the inorganic framework,

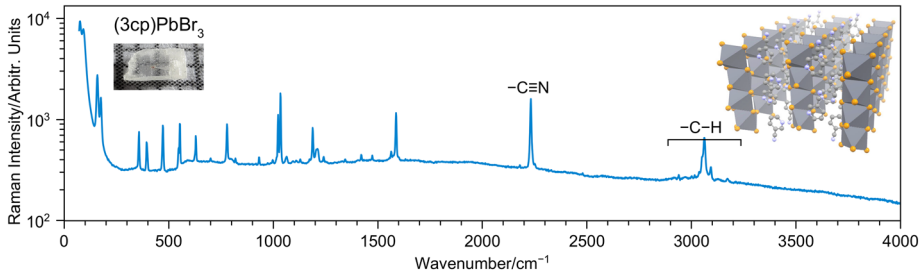

FIGURE 1 Experimental Raman spectrum of $(3cp)PbBr_3$ (log scale). Insets show $(3cp)PbBr_3$ photo and crystal structure.

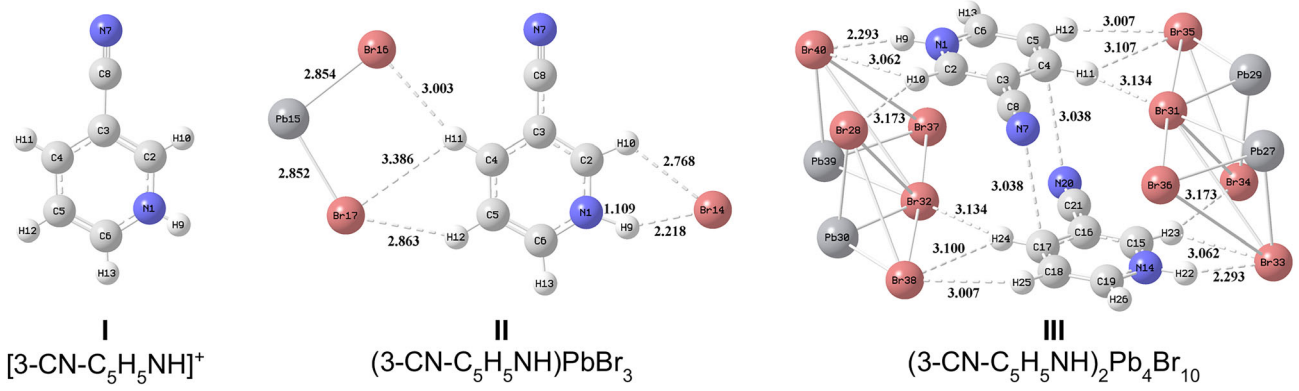

FIGURE 2 Studied cluster models: **I**—free cation (C_s symmetry), **II**—stoichiometric cluster (C_s symmetry), **III**—nanocluster (C_i symmetry). Atoms: dark grey—carbon, light gray—hydrogen, blue—nitrogen and red—bromine. Numbers denote the distance between atoms in Å.

all the peaks observed in the range of 150–3200 cm^{-1} refer to internal vibrations of (3cp) cations. To interpret this spectrum, three different models were calculated, which are fragments of the crystal structure obtained in XRD.[24]

Three studied cluster models are shown in Figure 2. Cluster **I** is the $(3cp)^+$ free cation obtained by protonating of the 3-cyanopyridine molecule. It has $N = 13$ atoms and belongs to the C_s point group characterised by a mirror plane through all atoms. Cluster **II** is the minimal stoichiometric cluster with formula $(3cp)PbBr_3$ coinciding with that of the actual material. For the same reason, the cluster is electrically neutral. Three bromine atoms and a lead atom were chosen so that cluster **II** also belongs to the point group C_s. The same mirror plane is also present in the crystal structure at room temperature.[24] Cluster **III** with formula $(3cp)_2Pb_4Br_{10}$ consists of the $(3cp)^+$ cations dimer and two $[Pb_2Br_5]^-$ fragments of different post-perovskite inorganic layers. This cluster is non-stoichiometric, electrically neutral and belongs to the C_i point group with the inversion center also present in the crystal structure. Next, we consider the results of DFT calculation for each of the models. For calculated Raman spectra the $C_1 = 0.924$ and $C_2 = 0.938$ scale factors were used for the 0–2500 cm^{-1} and >3000 cm^{-1} spectral regions, respectively.

3.1 | Cluster I—Free cation

Cluster geometry was fully optimised using wB97XD/def2SVP density functional. The absence of imaginary vibrational wavenumbers indicated that a local minimum had been reached. The symmetry analysis of the cation yield $3N - 6 = 33$ normal modes with in-plane (A') and out-of-plane (A'') vibrations ($\Gamma_{vib} = 23A' + 10A''$). Table 1 shows scaled calculated wavenumbers. All vibrations are both IR and Raman active. Calculated Raman spectra are shown in Figure 3 (red curve).

In the lowest wavenumber region, weak out-of-plane (A'') wagging (ω)–C–H vibrations and weak torsional (τ) vibrations of the pyridinium ring are located. In-plane (A') scissor (δ) and pendular (ρ) vibrations of the –C–H groups and ring are mostly located in the 1000–1500 cm^{-1} region. Among them, the most Raman-active modes are 1163.8, 994.6 and 969.0 cm^{-1}. The intense 1587.5 cm^{-1} mode corresponds to the stretching vibrations (υ) of –C=C– and –N=C–double bonds of the pyridinium ring. Most of these modes were unambiguously matched to experimental values in Table 1.

The high-wavenumber region of the spectra is depicted in Figure 4. The intense −C≡N triple bond stretching mode is located at 2242.7 cm^{-1} very close to the experimentally observed Raman line at 2234 cm^{-1}.

TABLE 1 Experimental and calculated (clusters **I** and **II**) wavenumbers.

No.	Symmetry	Experimental wavenumber/cm^{-1}	Scaled calculated wavenumbers/cm^{-1} (Raman intensity)		Assignment (with cluster number for different assignments)
			Cluster I	Cluster II	
ν_{33}	A'	3095 (w)	**3360.0 (73)**	–	υ(N1–H) **I**
ν_{32}	A'	**3065 (m)**	**3060.2 (144)**	**3056.8 (175)**	υ(C6–H) + υ(C5–H)
ν_{31}	A'	3051 (sh)	3051.2 (17)	**3044.2 (163)**	υ(C5–H) − υ(C6–H)
ν_{30}	A'	–	**3050.9 (81)**	**3005.2 (204)**	υ(C2–H) **I**/υ(C4–H) **II**
ν_{29}	A'	2940 (w)	**3036.0 (52)**	**2949.4 (102)**	υ(C4–H) **I**/υ(C2–H) **II**
ν_{28}	A'	**2234 (s)**	**2242.7 (285)**	**2237.2 (206)**	υ(C ≡ N)
ν'_{28}	A'	–	**–**	**2176.5 (333)**	υ(N1–H---Br) **II**
ν_{27}	A'	**1587 (s)**	**1587.6 (70)**	**1581.9 (48)**	υCC + υCN (ring stretch)
ν_{26}	A'	1565 (w)	1550.8 (9.9)	1538.6 (13)	υCC + υCN (ring stretch)
ν_{25}	A'	1475 (w)	1478.1 (2.9)	1431.9 (10)	δHCC + δHNC + υCC + υCN
ν_{24}	A'	1422 (w)	1390.3 (0.7)	1374.6 (4.1)	ρCH + υCC + υCN
ν_{23}	A'	1346 (w)	1281.3 (3.8)	**1257.5 (38)**	δHCN + δHCC + υCC-υCN
ν_{22}	A'	1243 (w)	1260.0 (3.1)	1225.3 (5.1)	ρCH + υCC + υCN
ν_{21}	A'	**1213 (m)**	1208.8 (5.3)	1184.1 (12)	δHCC + δHCN + υCN
ν_{20}	A'	**1190 (m)**	**1163.8 (25)**	**1147.5 (44)**	δHCC + υ(C–C) (cyano group)
ν_{19}	A'	1129 (w)	1120.5 (4.1)	**1107.0 (24)**	ρCH + υCC + υCN
ν_{18}	A'	1063 (w)	1051.1 (1.6)	1051.8 (8.0)	δHCC + ρCH + υCC
ν_{17}	A'	**1031 (s)**	**994.6 (21)**	**985.0 (58)**	υCC + υCN + ρCH (breathing)
ν_{16}	A''		972.4 (0.3)	1048.6 (11)	ωCH + τCCCC (bending)
ν_{15}	A'	997 (w)	**969.0 (23)**	981.5 (0.6)	δCNC + δCCC (stretching)
ν_{14}	A''	933 (w)	937.0 (0.1)	934.8 (2.0)	ωCH + ωNH + τCCCN (bending)
ν_{13}	A''		898.8 (1.5)	911.6 (9.5)	ωCH + ωNH + τCCCC (bending)
ν_{12}	A''	821 (w)	811.2 (1.1)	903.8 (7.1)	ωCH + ωNH
ν_{11}	A''	804 (sh)	748.9 (0.5)	783.4 (0.2)	τCCCC + τCCCN + ωCH + ωNH
ν_{10}	A'	**780 (m)**	**736.1 (8.7)**	**738.8 (24)**	δCCN + δCCC + υCC (cyano group)
ν_{9}	A''	702 (w)	635.2 (0.5)	658.1 (0.5)	ωCH + ωHN + bending
ν_{8}	A'	**630 (m)**	593.4 (2.8)	579.2 (2.8)	δCCC + δCNC
ν_{7}	A''	**553 (m)**	**532.1 (4.3)**	**555.1 (3.7)**	ωCCCC + ωNH + ωCH
ν_{6}	A'		510.4 (1.9)	514.5 (2.1)	δCCN + δCCC
ν_{5}	A'	**472 (m)**	**440.2 (4.4)**	**441.7 (4.5)**	δCCC + δCNC
ν_{4}	A''	**396 (m)**	370.5 (0.1)	389.6 (0.2)	τCCCN + τCCCC (bending)
ν_{3}	A''	**358 (m)**	343.9 (2.9)	**360.1 (3.3)**	τCCCC + τCCCN + δCCN (cyano group)
ν_{2}	A'	–	147.2 (3.4)	159.5 (3.2)	δCCN (cyano group)
ν_{1}	A''	–	136.0 (0.3)	141.2 (0.5)	τNCCC (bending)

Abbreviations: δ, ρ, scissor and pendular in-plane deformational vibrations, respectively; υ, stretching vibrations; ω, τ, wagging and torsional out-of-plane deformational vibrations, respectively; m, medium; sh, shoulder; s, strong; w, weak. The most intense modes are in bold.

Calculated –C–H stretching vibrations (Figure 4B, red curve) are lying above 2900 cm^{-1}. Compared to the spectrum of the 3-cyanopyridine molecule, the addition of a proton results in the emergence of pronounced –N–H stretching vibration. The calculation for a free cation (cluster **I**) gives the wavenumber of these vibrations as 3360 cm^{-1} (shown by the red arrow in Figure 4A). However, this vibration is not observed in the experimental spectrum (Figure 4A). This is due to the fact that the –N–H vibration wavenumber is sufficiently transformed

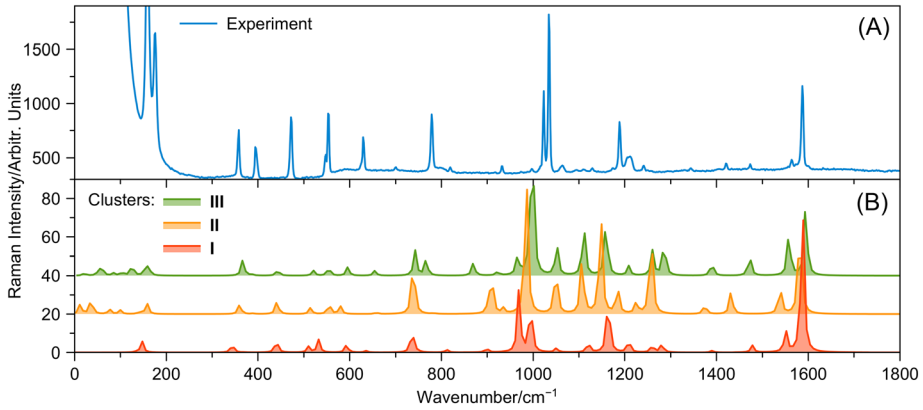

FIGURE 3 Experimental (A) and calculated (B) Raman spectra for the 0–1800 cm^{-1} region.

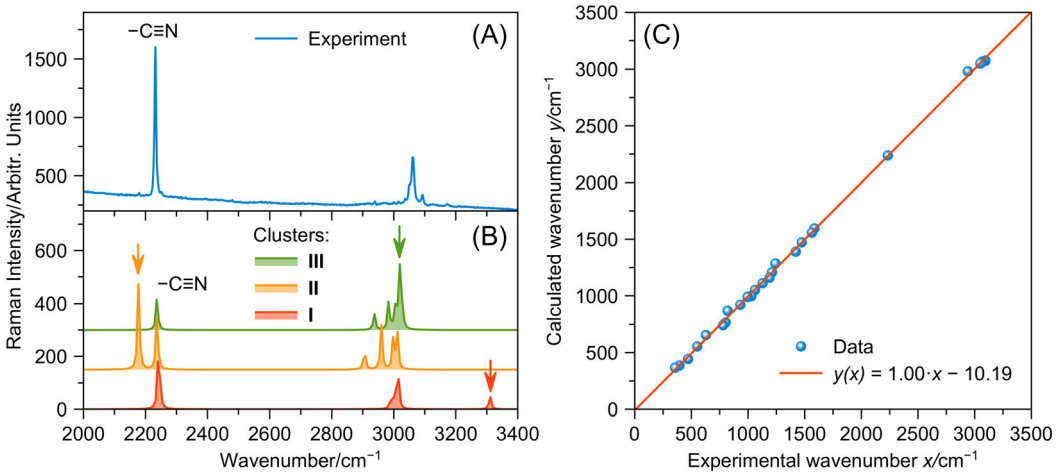

FIGURE 4 Experimental (A) and calculated (B) Raman spectra for the 2000–3400 cm^{-1} region. Arrows denote the –N–H stretching vibration. (C) Correlation of experimental and calculated wavenumbers for cluster **III**.

under the action of the crystalline environment in comparison with the free cation **I**. For this reason, the calculation of a larger cluster is necessary.

3.2 | Cluster II—Stoichiometric cluster

The (3cp)$PbBr_3$ cluster **II** was partially optimised with the fixed position of inorganic atoms. As in the case of cluster **I**, only 13 atoms of (3cp) cation were not fixed in cluster **II**. Calculated wavenumbers for cluster **II** are presented in Table 1 and the calculated Raman spectrum is shown in Figure 3B and Figure 4B (orange curve). Modes in the 0–1800 cm^{-1} region experience only minor shifts and some increase in the Raman activity. The pronounced –C ≡ N stretching mode remains practically at the same wavenumber as in cluster **I** and experiment.

The approximate local crystal field created by the atoms of the inorganic framework included in cluster **II** has a significant effect on the wavenumbers of hydrogen stretching vibrations.

The most pronounced shift is observed for the –N–H···Br vibration $\nu'_{28} = 2176.5$ cm^{-1} in cluster **II** in comparison with –N–H vibration $\nu_{33} = 3360.0$ cm^{-1} for free cation in cluster **I**. The decrease in wavenumber by almost 1200 cm^{-1} is associated with the attraction of hydrogen to the bromine atom and a decrease in the strength of the bond with nitrogen. This conclusion is supported by the analysis of the bond lengths and bond orders for constituent atoms in Tables 2 and 3. The Br14···H9 bond in cluster **II** has a bond length of 2.218 Å and a bond order of 0.381. The appearance of this bond leads to an increase in the N1–H9 bond length from 1.021 Å for cluster **I** to 1.109 Å for cluster **II**, and a simultaneous drop in the bond order from 0.900 to 0.693. Accounting for the local crystalline environment also leads to the weak decrease (∼100 cm^{-1}) of the ν_{29} wavenumber. This is the stretching vibration of the H10 hydrogen connected to the C2 ring carbon.

Such a strong decrease in the –N–H stretching vibration wavenumber (shown by the orange arrow in Figure 4A) should move it close to the ν_{28} vibration

TABLE 2 Bond lengths and bond orders for organic cation bonds.

Group	Bond	Bond length, Å			Bond order		
		I	II	III	I	II	III
Ring	N1≃C6	1.347	1.356	1.343	1.303	1.320	1.306
Ring	N1≃C2	1.343	1.333	1.334	1.323	1.411	1.359
Ring	C2≃C3	1.391	1.397	1.392	1.421	1.342	1.397
Ring	C3≃C4	1.405	1.400	1.402	1.371	1.402	1.370
Ring	C4≃C5	1.394	1.395	1.393	1.394	1.387	1.400
Ring	C5≃C6	1.383	1.381	1.381	1.452	1.438	1.442
Substituent	C3≃C8	1.436	1.438	1.436	1.090	1.083	1.103
Cyano	N7≡C8	1.115	1.156	1.156	3.011	3.019	2.964
Protonation	N1–H9	1.021	1.109	1.038	0.900	0.693	0.832
	C2–H10	1.091	1.100	1.097	0.956	0.933	0.939
	C4–H11	1.092	1.094	1.092	0.971	0.966	0.967
	C5–H12	1.090	1.090	1.090	0.964	0.963	0.963
	C6–H13	1.091	1.091	1.089	0.955	0.971	0.962

Note: For atom numbers see Figure 2. In cluster **III** bonds for the second cation are the same due to the symmetry.

TABLE 3 Bond lengths and bond orders for hydrogen-halogen bonds.

Bond	Bond length, Å		Bond order	
	II	III	II	III
Br14/Br40···H9	2.218	2.293	0.381	0.172
Br14/Br40···H10	2.768	3.062	0.131	0.026
Br17/Br35···H11	3.386	3.100	0.019	0.044
Br17/Br35···H12	2.863	3.007	0.037	0.033
Br16/Br31···H11	3.003	3.134	0.052	0.016
–/Br28···H10	–	3.174	–	0.075

Note: For bromine atoms numbers are given for clusters **II**/**III**. For atom numbers see Figure 2.

corresponding to the –C ≡ N stretching. However, this contradicts the experimental observation depicted in Figure 4A, where only one peak is observed in the 2000–2800 cm^{-1} wavenumber range. Thus, both the model of a free cation in cluster **I** and the first approximation of the crystal field in cluster **II** do not allow one to describe –N–H vibration correctly, and a bigger cluster is required to a more accurately model the crystal field.

3.3 | Cluster III—Nanocluster

The $(3cp)_2Pb_4Br_{10}$ cluster **III** was partially optimised with the fixed position of inorganic atoms, C2 and C15 atoms in order to keep the cluster structure. Cluster **III** consists of two organic cations connected by the inversion operation of the point group C_i. Group-theoretic analysis shows that vibrations of two symmetries are possible: A_u, which is only IR-active, and A_g, which is only Raman-active. The A_g vibrations are symmetrical with respect to the center of inversion and could be represented as in-phase vibrations of two organic cations. The number of internal vibrational modes in cluster **III** is doubled compared to clusters **I** and **II**. However, the number of normal modes observed in the Raman spectra should remain the same −33, since only half of 66 modes belong to the A_g symmetry. Scaled calculated wavenumbers for cluster **III** are presented in Table 4, and the calculated Raman spectrum is shown in Figure 3B and Figure 4B (green curve). There are two cluster **III** modes (A_g and A_u) for each free cation mode in Table 4.

The main feature of cluster **III** compared to cluster **II** is a more accurate consideration of the local environment of the bromine anion. The presence of lead cation Pb^{2+} and an additional bromine anion Br^- leads to the redistribution of the electron density on the bromine of interest and the decrease of the H···Br bond strength. This leads to the increase of the (N1–H···Br) wavenumber from $\nu'_{28} = 2176.5$ cm^{-1} in cluster **II** to $\nu_{32}(A_g)$ = 3064.0 cm^{-1} in cluster **III**. This brings this N–H vibration to the region of C–H stretching vibrations (shown by the green arrow in Figure 4A). The experimental observations in Figure 4B support this result and verify the correctness of the cluster **III** construction procedure.

The –N–H···Br interaction raises the question of the presence of the H···Br hydrogen bond in this material.

TABLE 4 Experimental and calculated (cluster **III**) wavenumbers.

No. of free cation vibration mode	Assignment	Symmetry	Scaled calculated wavenumber/cm^{-1} (Raman intensity) Cluster III	Experimental wavenumber/cm^{-1}
ν_{33}	υ(C6–H) + υ(C5–H)	A_g	**3073.8 (197)**	3095 (w)
		A_u	3073.8 (0)	–
ν_{32}	υ(N1–H---Br)	A_g	**3064.0 (699)**	**3065 (m)**
		A_u	3063.6 (0)	–
ν_{31}	υ(C5–H) − υ(C6–H)	A_g	**3050.0 (207)**	3051 (sh)
		A_u	3050.2 (0)	–
ν_{30}	υ(C4–H)	A_g	**3029.0 (294)**	–
		A_u	3029.0 (0)	–
ν_{29}	υ(C2–H---Br)	A_g	**2981.6 (171)**	2940 (w)
		A_u	2981.7 (0)	–
ν_{28}	υ(C≡N)	A_g	**2237.3 (276)**	**2234 (s)**
		A_u	2237.1 (0)	–
ν_{27}	υCC + υCN + δHCC + δHNC	A_g	**1594.5 (71)**	**1587 (s)**
		A_u	1595.1 (0)	–
ν_{26}	υCN + υCC + δHCC + δHNC	A_g	**1558.1 (44)**	1565 (w)
		A_u	1558.3 (0)	–
ν_{25}	δHCC + δHNC + υC=C	A_g	**1472.2 (21)**	1475 (w)
		A_u	1472.3 (0)	–
ν_{24}	δHNC + δHCC + υCC − υCN	A_g	**1390.0 (13)**	1422 (w)
		A_u	1390.2 (0)	–
ν_{23}	υC=C − υCC + δHNC + δHCC	A_g	**1285.8 (34)**	1243 (w)
		A_u	1285.3 (0)	–
ν_{22}	ρCH + υCC – υCN	A_g	**1260.5 (22)**	–
		A_u	1260.2 (0)	–
ν_{21}	δHCN + δHCC + υCN	A_g	**1208.5 (8.2)**	**1213 (m)**
		A_u	1208.3 (0)	–
ν_{20}	υCC (cyano group) + ρCH	A_g	**1159.2 (52)**	**1190 (m)**
		A_u	1159.2 (0)	–
ν_{19}	ρCH (ring)	A_g	**1110.4 (46)**	1129 (w)
		A_u	1110.6 (0)	–
ν_{18}	ρCH + υCC + υCN	A_g	**1051.5 (28)**	1063 (w)
		A_u	1050.9 (0)	–
ν_{17}	ωNH + ωCH	A_g	**998.4 (127)**	**1031 (s)**
		A_u	998.3 (0)	–
ν_{16}	υCC + υCN + ωNH + ωCH	A_g	**991.5 (12)**	997 (w)
		A_u	991.4 (0)	–
ν_{15}	ωCH + τCCCC (bending)	A_g	**969.4 (4.3)**	–
		A_u	969.1 (0)	–
ν_{14}	δCCN + δCCC (ring)	A_g	**965.2 (12)**	–
		A_u	965.2 (0)	–

(Continues)

TABLE 4 (Continued)

No. of free cation vibration mode	Assignment	Symmetry	Scaled calculated wavenumber/cm^{-1} (Raman intensity) Cluster III	Experimental wavenumber/cm^{-1}
ν_{13}	ωNH + ωCH + τCCCC	A_g	**922.7 (3.1)**	933 (w)
		A_u	922.6 (0)	–
ν_{12}	ωCH + ωNH + τCCCN	A_g	**869.9 (10)**	821 (w)
		A_u	869.8 (0)	–
ν_{11}	ωCH + ωNH + τCCCC	A_g	**766.8 (13)**	804 (sh)
		A_u	766.8 (0)	–
ν_{10}	δCCN + υCC (cyano group)	A_g	**742.6 (19)**	**780 (m)**
		A_u	742.3 (0)	–
ν_9	τCCCC + τCCCN + ωCH + ωNH	A_g	**654.8 (3.7)**	**630 (m)**
		A_u	655.7 (0)	–
ν_8	δCCC + δCNC (ring)	A_g	**595.8 (6.4)**	–
		A_u	595.8 (0)	–
ν_7	τCCCN + τCCCC	A_g	**554.4 (6.5)**	**553 (m)**
		A_u	554.0 (0)	–
ν_6	δCCN (cyano group)	A_g	**520.8 (3.6)**	–
		A_u	520.1 (0)	–
ν_5	δCCC + δNCC (ring)	A_g	**443.1 (4.5)**	**472 (m)**
		A_u	443.7 (0.0)	–
ν_4	τCCCN + τCCCC	A_g	**385.8 (0.8)**	**396 (m)**
		A_u	385.9 (0)	–
ν_3	τCCCC + τCCCN + δCCN	A_g	**367.0 (11)**	**358 (m)**
		A_u	364.9 (0)	–
ν_2	δCCN (cyano group)	A_g	**162.4 (4.0)**	–
		A_u	170.9 (0)	–
ν_1	τNCCC (bending)	A_g	**155.7 (7.2)**	–
		A_u	162.1 (0)	–

Abbreviations: δ, ρ, scissor and pendular in-plane deformational vibrations, respectively; υ, stretching vibrations; ω, τ, wagging and torsional out-of-plane deformational vibrations, respectively; m, medium; sh, shoulder; s, strong; w, weak. The most intense modes are in bold.

According to the classification presented in earlier papers,[27,28] the distance between hydrogen and acceptor (bromine in this case) below 3 Å could potentially be considered as hydrogen bonding. Bonds with hydrogen–acceptor distances above 2.2 Å and donor–hydrogen–acceptor bond angles far below 180° are considered as weak hydrogen bonds. The experimentally supported modeling of cluster **III** yields the 2.293 Å bond length for H9···Br14, so it should fall in the weak hydrogen bonds class. However, the rather short distance between hydrogen and two more bromide anions (Br34 and Br36) may be considered as bi- or tri-furcated hydrogen bonds with H9···Br14 bond being the major component. Thus, the question of the presence of a hydrogen bond and its role in stabilising the structure of this perovskite-like halide remains open.

TABLE 5 Bond lengths and bond orders for stacking interaction bonds in cluster **III**.

Bond	Bond length, Å	Bond order
N7·····C17	3.038	0.019
N7·····H24	2.900	0.005

Note: For atom numbers see Figure 2.

According to calculations, the stacking interaction between rings of neighboring organic cations is relatively weak (see Table 5). Thus, the role of this interaction in

the formation of the layered structure of low-dimensional post-perovskite seems to be insignificant.

The calculation performed is in good agreement with experiment. Figure 4C shows the linear correlation between experimental wavenumbers and wavenumbers calculated for cluster **III**. The correlation coefficient is $R^2 = 0.9992$. For most of the internal vibrations, it is sufficient to consider the model of a free cation. The correct account of the crystalline environment for hydrogen atoms (primarily located on nitrogen), requires the construction of sufficiently large clusters. An important condition for the construction of such clusters is not only the inclusion of the nearest halogen anions but also of their environment to provide their correct electronic configuration.

4 | CONCLUSION

In this work, we have studied the vibrations of the $(3cp)^+$ molecular cation in the $(3cp)PbBr_3$ halide post-perovskite. In order to explain the observed Raman spectrum, three cluster models were suggested for DFT modeling: free cation, minimal stoichiometric cluster and nanocluster. Low-wavenumber internal vibrations of the cation can be satisfactorily explained even in the free cation model. However, for a correct description of the stretching vibrations with hydrogens, it is essential to take into account the crystal field. To take this field into account, it is not enough to introduce only the halogen anion, since the strong bond between halogen and hydrogen leads to an excessive decrease in the wavenumber of the N–H stretching vibration. The second and more correct approximation is the inclusion of the nearest environment of the halogen anion in the cluster. In this case, the calculation results coincide with experimental observations. This cluster approach can be used to calculate vibrations in other halide perovskites and their analogues. A comparison of the simulation results with the experiment could be used for finding the actual position of the hydrogen in the crystal structure, which cannot be determined by standard X-ray diffraction methods. The relatively small distance between hydrogen and halogen also raises the question of the magnitude of the hydrogen bond, the possibility of its bi- and tri-furcation, and its role in stabilising the crystal structure of the material.

ACKNOWLEDGEMENTS

This research was supported by the Russian Science Foundation (Project No. 22-22-00437). This work was carried out on the equipment of the SPbU Resource Centers 'Center for Optical and Laser Materials Research' and 'Geomodel'. We are grateful to the Computing Center of St. Petersburg State University, http://www.cc.spbu.ru, for calculation facilities.

CONFLICT OF INTEREST STATEMENT

The authors declare no conflict of interest.

ORCID

Anna Yu Samsonova https://orcid.org/0000-0003-4303-3091

REFERENCES

[1] A. Kojima, K. Teshima, Y. Shirai, T. Miyasaka, *J. Am. Chem. Soc.* **2009**, *131*, 6050.
[2] M. P. Mamaeva, A. Y. Samsonova, A. O. Murzin, O. A. Lozhkina, A. A. Murashkina, N. I. Selivanov, Y. V. Kapitonov, *J. Phys. Chem. C* **2022**, *126*, 19816.
[3] A. O. Murzin, B. V. Stroganov, C. Günnemann, S. B. Hammouda, A. V. Shurukhina, M. S. Lozhkin, A. V. Emeline, Y. V. Kapitonov, *Adv. Opt. Mater.* **2020**, *8*, 2000690.
[4] J. Chen, H. Xiang, J. Wang, R. Wang, Y. Li, Q. Shan, X. Xu, Y. Dong, C. Wei, H. Zeng, *ACS Nano* **2021**, *15*, 17150.
[5] R. S. Nazarov, I. A. Solovev, A. O. Murzin, N. I. Selivanov, J. Even, A. V. Emeline, Y. V. Kapitonov, *Phys. Rev. B* **2022**, *105*, 245202.
[6] Q. A. Akkerman, L. Manna, *ACS Energy Lett.* **2020**, *5*, 604.
[7] L. Mao, C. C. Stoumpos, M. G. Kanatzidis, *J. Am. Chem. Soc.* **2019**, *141*, 1171.
[8] N. I. Selivanov, R. Kevorkyants, A. V. Emeline, C. C. Stoumpos, *Materials* **2023**, *16*, 353.
[9] N. I. Selivanov, A. A. Murashkina, R. Kevorkyants, A. V. Emeline, D. W. Bahnemann, *Dalton Trans.* **2018**, *47*, 16313.
[10] N. I. Selivanov, Y. A. Rozhkova, R. Kevorkyants, A. V. Emeline, D. W. Bahnemann, *Dalton Trans.* **2020**, *49*, 4390.
[11] M. Shin, S.-W. Nam, A. Sadhanala, R. Shivanna, M. Anaya, A. Jiménez-Solano, H. Yoon, S. Jeon, S. D. Stranks, R. L. Z. Hoye, B. Shin, *ACS Appl. Energy Mater.* **2020**, *3*, 192.
[12] X. Li, T. T. H. Do, A. Granados del Águila, Y. Huang, W. Chen, Q. Xiong, Q. Zhang, *Chem. Asian J.* **2018**, *13*, 3185.
[13] M. Ben Haj Salah, J. Tessier, N. Mercier, M. Allain, A. Leblanc, X. Che, C. Katan, M. Kepenekian, *Crystals* **2021**, *11*, 1570.
[14] G.-E. Wang, G. Xu, B.-W. Liu, M.-S. Wang, M.-S. Yao, G.-C. Guo, *Angew. Chem. Int. Ed.* **2016**, *55*, 514.
[15] M. D. Smith, B. A. Connor, H. I. Karunadasa, *Chem. Rev.* **2019**, *119*, 3104.
[16] J.-C. Blancon, A. V. Stier, H. Tsai, W. Nie, C. C. Stoumpos, B. Traoré, L. Pedesseau, M. Kepenekian, F. Katsutani, G. T. Noe, J. Kono, S. Tretiak, S. A. Crooker, C. Katan, M. G. Kanatzidis, J. J. Crochet, J. Even, A. D. Mohite, *Nat. Commun.* **2018**, *9*, 2254.
[17] M. Hirasawa, T. Ishihara, T. Goto, *J. Physical Soc. Japan* **1994**, *63*, 3870.
[18] B. Dhanabalan, Y.-C. Leng, G. Biffi, M.-L. Lin, P.-H. Tan, I. Infante, L. Manna, M. P. Arciniegas, R. Krahne, *ACS Nano* **2020**, *14*, 4689.
[19] S. N. Lavan, A. M. Sanni, A. S. Rury, Z.-F. Liu, *J. Phys. Chem. C* **2021**, *125*, 223.

[20] S. Toda, E. Wei-Guang Diau, S. Shigeto, *J. Phys. Chem. C* **2021**, *125*(51), 27996.
[21] Y. Zhou, H. F. Garces, N. P. Padture, *Front. Optoelectron.* **2016**, *9*, 81.
[22] R. A. Evarestov, V. P. Smirnov, *Springer series in sold state sciences*, Vol. 108, Springer, New York **1997**.
[23] X. Yuan, K. Luo, N. Liu, X. Ji, C. Liu, J. He, G. Tian, Y. Zhao, D. Yu, *Phys. Chem. Chem. Phys.* **2018**, *20*, 20779.
[24] N. I. Selivanov, A. Y. Samsonova, R. Kevorkyants, I. V. Krauklis, Y. V. Chizhov, B. V. Stroganov, M. E. Triantafyllou-Rundell, D. W. Bahnemann, C. C. Stoumpos, A. V. Emeline, Y. V. Kapitonov, *Adv. Funct. Mater.* **2021**, *31*, 2102338.
[25] A. Y. Samsonova, I. V. Krauklis, Y. V. Chizhov, N. I. Selivanov, A. V. Emeline, Y. V. Kapitonov, *J. Phys. Chem. Lett.* **2023**, *14*, 3445.
[26] M. J. Frisch, G. W. Trucks, H. B. Schlegel, G. E. Scuseria, M. A. Robb, J. R. Cheeseman, G. Scalmani, V. Barone, G. A. Petersson, H. Nakatsuji, X. Li, M. Caricato, A. V. Marenich, J. Bloino, B. G. Janesko, R. Gomperts, B. Mennucci, H. P. Hratchian, J. V. Ortiz, A. F. Izmaylov, J. L. Sonnenberg, D. Williams-Young, F. Ding, F. Lipparini, F. Egidi, J. Goings, B. Peng, A. Petrone, T. Henderson, D. Ranasinghe, V. G. Zakrzewski, J. Gao, N. Rega, G. Zheng, W. Liang, M. Hada, M. Ehara, K. Toyota, R. Fukuda, J. Hasegawa, M. Ishida, T. Nakajima, Y. Honda, O. Kitao, H. Nakai, T. Vreven, K. Throssell, J. A. Montgomery, Jr., J. E. Peralta, F. Ogliaro, M. J. Bearpark, J. J. Heyd, E. N. Brothers, K. N. Kudin, V. N. Staroverov, T. A. Keith, R. Kobayashi, J. Normand, K. Raghavachari, A. P. Rendell, J. C. Burant, S. S. Iyengar, J. Tomasi, M. Cossi, J. M. Millam, M. Klene, C. Adamo, R. Cammi, J. W. Ochterski, R. L. Martin, K. Morokuma, O. Farkas, J. B. Foresman, D. J. Fox, *Gaussian 16; Revision, A.03*; Gaussian, Inc.: Wallingford, CT, USA, **2016**.
[27] T. Steiner, *Angew. Chem. Int. Ed.* **2002**, *41*, 48.
[28] G. A. Jeffrey, *An Introduction to Hydrogen Bonding*, Oxford University Press, Oxford **1997**.

How to cite this article: I. V. Krauklis, A. Y. Samsonova, N. I. Selivanov, Y. V. Kapitonov, Y. V. Chizhov, *J Raman Spectrosc* **2023**, 1. https://doi.org/10.1002/jrs.6618